Image Cover Sheet

CLASSIFICATION	SYSTEM NUMBER
UNCLASSIFIED	503450

TITLE

CAVITATION PERFORMANCE OF PROPELLER BLADE ROOT FILLETS

System Number:

Patron Number:

Requester:

Notes:

DSIS Use only:

Deliver to:

Cavitation Performance of Propeller Blade Root Fillets

J.L. Kennedy (Defence Research Establishment Atlantic), **D.L. Walker** (Marineering Ltd.) **J.M. Doucet** (Memorial University of Newfoundland) and **T. Randell** (Institute for Marine Dynamics)

ABSTRACT

Propeller cavitation is a potent source of ship noise and vibrations, poses a risk of blade erosion and is normally to be avoided. The root of a propeller blade, where it joins the hub or palm, is normally fitted with a fillet of some sort. The fillet is primarily designed to reduce stress concentrations with little regard to hydrodynamic performance. At present there is little information available on the fillet's effects on propeller root cavitation. This paper presents the results of an experimental study of the effect of fillet design on blade root cavitation.

In the study, twelve wing/body intersections were used to model typical blade/hub intersections on a propeller. Eight models used a flat plate to model the hub and four modelled the hub using a NACA foil section. The models were sufficiently large to permit testing in the Institute for Marine Dynamics' cavitation tunnel at Reynolds numbers representative of full scale. The fillets tested covered a broad range of geometry and permitted direct comparison of the effect of fillet geometry on cavitation performance. By comparing the results of tests with the two hub models, the role of the hub shape was also briefly examined. The results allow a propeller designer to qualitatively discriminate between fillets for improved root fillet cavitation performance. The consequences of this for propeller designs are briefly reviewed.

NOMENCLATURE

- **P** - Tunnel pressure
- $\mathbf{P_v}$ - Vapour pressure of water
- $\mathbf{P_{Atm}}$ - Atmospheric pressure
- **T** - Blade section maximum thickness
- **V** - Tunnel velocity
- **X/C** - Blade section chord fraction
- α - Gas content
- α_s - Saturated gas content
- θ - Angle of attack
- ρ - Density of water
- σ - Cavitation number $(\mathbf{P} - \mathbf{P_v}) / 0.5\rho\mathbf{V}^2$
- σ_i - Cavitation number at inception

INTRODUCTION

Propeller cavitation is a potent source of ship noise and vibrations, and poses a risk of blade erosion. It is normally to be avoided. In the past tip vortex and sheet cavitation at outer radii were the most problematic, but advances in propeller design have pushed the inception speeds of these steadily higher. Consequently, blade root fillet cavitation has become a more critical type.

Blade root fillets are designed to reduce stress concentrations. Classification societies (Lloyd's Register, 1982, Det Norske Veritas, 1993) give rules for single radius fillets but allow the option of more complex forms that reduce stress concentrations considerably. Compound fillets, made up of two radii based on blade maximum thickness, typically 3T and T/3, approximate low stress fillet shapes. Little is known about the relative cavitation performance of any such fillet shapes.

The hydrodynamics of blade root fillets depends on the geometry of the blade, the fillet and the hub. We tested one blade shape, twelve fillets and two hub shapes. We were interested in constant radius cylinders and approximately spherical hub shapes.

It was not practical to build a set of model propellers fitted with the above range of test fillets. The tests were therefore conducted on wing/body intersection models in rectilinear flow. These could be built at a large scale, consequently the Reynolds number of the tests was of the same order of magnitude as found on ships of interest.

On the wing/body test setup, the cylindrical propeller hub was modelled by a plane and the spherical propeller hub was modelled by a foil shape. In this latter case, a NACA 0020 foil was used as its minimum pressure matched the minimum pressure of a spherical hub of

interest. In this paper the names 'planar hub' and 'NACA hub' refer to the models of the cylindrical and spherical propeller hubs respectively. The propeller blade was modelled by a constant chord, uncambered, untwisted wing section, as that was relatively inexpensive to build. The blade was swept forward at 45 degrees to the hub, modeling the angle between blade and hub at the leading edge on some propellers.

Classification society rules provide no guidance on how the fillet size may vary around the blade foot. One option is to maintain the same size of fillet from leading to trailing edge. We mainly investigated models with these same-size fillets, including three with single radii, two with compound radii, one with an elliptic shape, and one with no fillet. We also tested one single-radius fillet model that varied in size around the blade foot.

All fillet models were tested at angles of attack up to seven degrees to the free stream. This goes somewhat beyond the angle normally used by propeller designers, but it accentuates the cavitation effects.

TEST MODEL GEOMETRY

The fillet models were designed using a PC based CAD/CAM program called Surfcam. Non-uniform rational B-spline surfaces were developed for each fillet and tool paths were generated for numerically controlled (NC) machining. The models were milled from a high density polyurethane foam known commercially as Ren Shape™450. This material was chosen since it is an isotropic material which provides excellent machinability and surface finish combined with high stability and stiffness. With the exception of the planar hub section, all of the parts were machined using a custom designed 5-axis NC milling machine located at IMD.

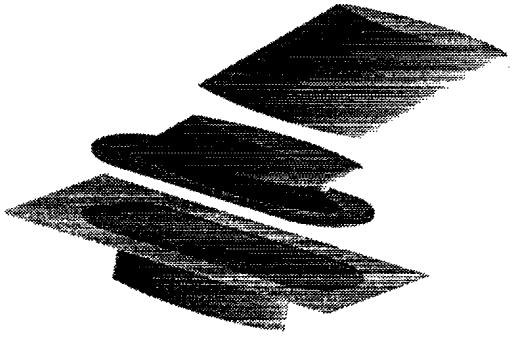

Figure 1: Test Model Components

Each test model consisted of three sections: a blade section; an interchangeable fillet section; and, a hub section; as shown in Figure 1. The fillet section fitted between the root and hub sections and its surface was blended tangent to both of them. The sections were fit together, as shown in Figure 2, over an internal steel backbone which attached to the test apparatus.

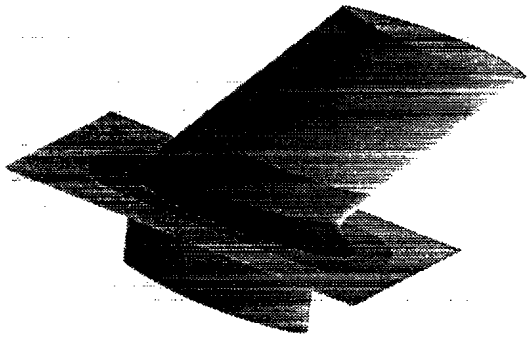

Figure 2: Test Model Components Assembled

Blade Section

The blade section was defined by a symmetrical NACA 066 (Mod) foil section with a thickness to chord length ratio of 0.25. This section is shown in Figure 3. The blade section was extruded in a straight line raked 45 degrees from vertical to form the surface. This blade section was common to all model configurations.

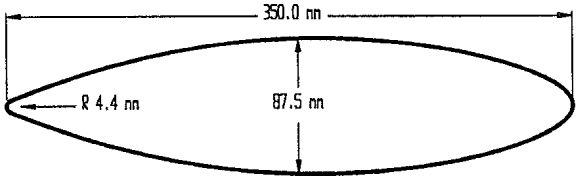

Figure 3: Blade Foil Section

Hub Sections

Two hub shapes were modelled: a planar hub (the lowest component in Figure 1) to represent a cylindrical propeller hub, and a NACA hub (Figure 4) to represent a spherical shaped propeller hub. The leading edge of the planar hub extended 150 mm ahead of the blade section at the root. It was fabricated from aluminium and did not require NC machining. The NACA 0020 shaped hub section had a chord length of 500 mm. The leading edge of this hub extended 75 mm ahead of the blade section at the root. It was NC milled from Ren Shape™450.

Figure 4: NACA Hub Section

Fillet Sections

These sections consisted of surfaces which blended the blade section into the hub sections. Depending on the size and extent of the fillet surfaces these sections also

contained parts of the blade and hub surfaces. The main defining parameter for all of the fillet geometries considered is the blade root section's maximum thickness, T. Several distinct types of fillet surfaces were modelled, as well as two with no fillet.

Single Radius Fillet

The surfaces used to define the single radius fillet sections were generated using automatic fillet surface creation functions within Surfcam. These functions generated a fillet of constant radius, between two surfaces. In these cases the two surfaces were the blade and the hub. For the planar hub three different fixed-radius fillet sections were produced with radii of T/2, T/3, and T/4. In this paper the test models with these single fillet radii are referred to by the names 'T/2', 'T/3', and 'T/4' respectively. For the NACA hub only the T/3 section was produced. Three views of the T/3 fillet section for the planar hub are shown in Figure 5. The lower left view is of the leading edge and the lower right view is of the trailing edge.

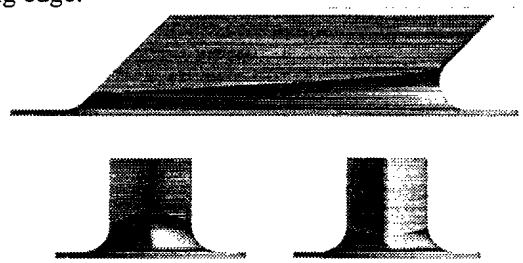

Figure 5: T/3 Single Radius Fillet - Planar Hub

In the case of the T/2 section the large size of the fillet caused the leading edge of the surface to wrap around on itself. This resulted in a sharp leading edge, compared to the rounded leading edge for the other fillet models.

Compound Radius Fillet

This case presented the most difficulty in creating the model, particularly in the case of the NACA hub model. Each fillet cross-section consisted of two arcs of different radii, nT and T/n, where n is a scaling ratio. The two arcs blend together at a common tangency point. The fillet geometry definition for n = 3 is shown in Figure 6.

There was no built-in surface creation function in Surfcam for these compound radius fillet surfaces. Therefore, a set of 20 cross-sections, over which the surfaces could be fit, was created. Each of the 20 cross-sections used was defined in a unique construction plane situated at spline node points on the intersection curve between the blade and hub surfaces. The construction plane for each cross-section was defined by two vectors located at each spline node point. The first vector was parallel to the ruling lines, at constant blade chord fraction, which defined the blade section. This vector, always at 45 degrees to vertical, was the same for all construction planes. The second vector was defined by the normal to the blade surface at the spline node points, along the intersection curve.

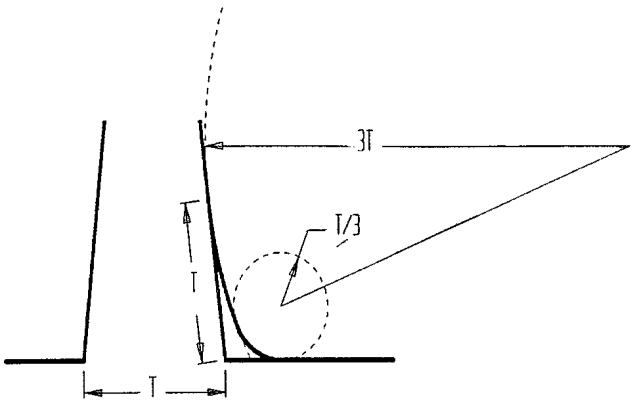

Figure 6: 3T-T/3 Fillet Definition

The arcs that form the cross-sections were blended tangent to curves defined by the intersection of the construction plane with both the blade and hub surfaces. In the case of the planar hub these were always straight lines. However, in the case of the NACA hub, the intersection with the hub surface was a compound curve that had a different shape at each spline node point. Figure 7 shows the cross-sections used to define the fillet surfaces as they are distributed around the blade/hub intersection curve for the NACA hub section.

Figure 7: Cross-sections for Compound Radius Fillet Surfaces

After all the cross-sections had been defined, the fillets were created by fitting surfaces over the regions with the same fillet radius. As a result two surfaces were generated for each fillet section. The upper surface, with radius nT, blends between the blade surface and the common tangency curve between the two fillet surfaces. The lower surface, with radius T/n, blends between the

common tangency curve and the hub surface. For the planar hub two different fillet models, with $n = 3$ and $n = 4$, were produced. For the NACA hub only the $n = 3$ fillet was produced.

In this paper the compound fillet test models with $n = 3$ and $n = 4$, are referred to by the names 'T/3-compound', and 'T/4-compound' respectively. Three views of the T/3-compound fillet section are shown in Figure 8 for the planar hub, and in Figure 9 for the NACA hub.

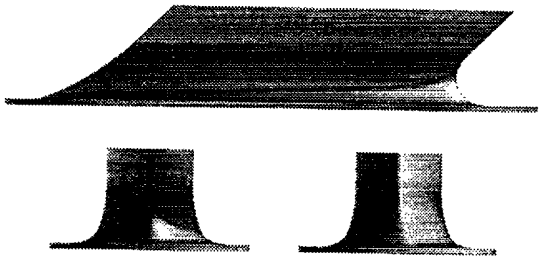

Figure 8: T/3-compound Fillet, Planar Hub

Figure 9: T/3-compound Fillet, NACA Hub

Elliptical Fillet

The technique used to create the elliptical fillet was similar to that used to develop the compound radius fillet.

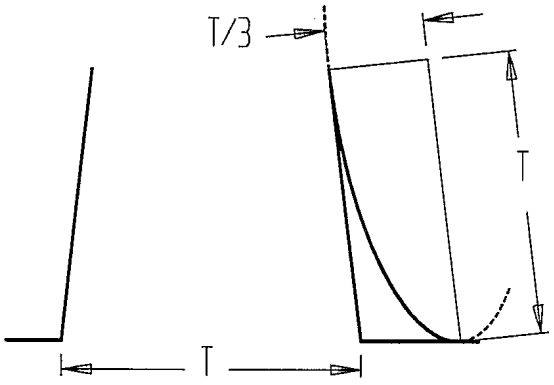

Figure 10: Elliptical Fillet Definition

An elliptical section was developed for each of the construction planes around the base of the blade root. The ellipse was aligned with the major axis, of length 2T, parallel to the ruling lines of the blade surface. The section geometry definition is shown in Figure 10.

The elliptical fillets were only produced for the planar hub. In this paper this fillet test model was referred to by the name 'T/3-elliptic'. Three views of this T/3-elliptic fillet section are shown in Figure 11.

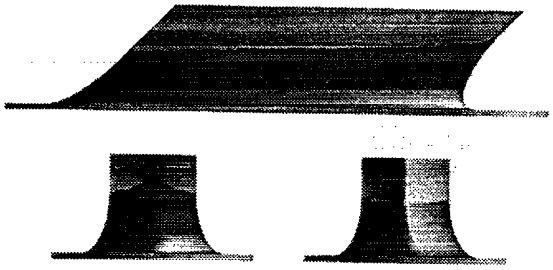

Figure 11: Elliptical Fillet, Planar Hub

No Fillet

In addition to the fillet sections, a section with no fillet was built for each of the two hubs. In these cases a blade section was put in place of the fillet section. In this paper these test models are referred to by the name 'No fillet'. Three views of the No fillet section for the NACA hub are shown in Figure 12.

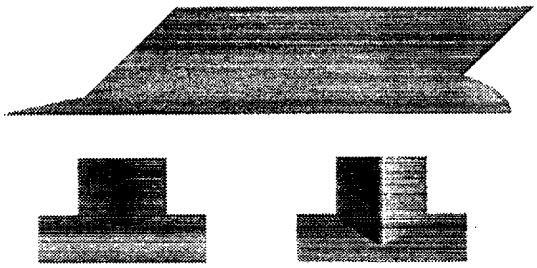

Figure 12: No fillet, NACA Hub

Variable Radius Fillet

Surfcam also provided a function for creating fillet surfaces where the single fillet radius varies in size along the intersection. The routines create this variable radius fillet by having the user define a distribution of discrete radii at fixed points along the intersection curve between the blade and hub surfaces. The program blends between the points at which discrete fillet radius values are defined to create a smooth, continuous, fillet surface.

The distribution of radii for the fillet surface we modelled was defined as: T/3 at the 0.5 chord point on the blade section; 80% of T/3 at the 0.25 and 0.75 chord points; and as 5 mm at the leading and trailing edges. Variable radius fillet sections were produced for both the planar and NACA hub models.

In this paper these variable radius fillet test models are referred to by the name 'T/3-variable'. Three views of the T/3-variable fillet section are shown in Figure 13 for the planar hub and in Figure 14 for the NACA hub.

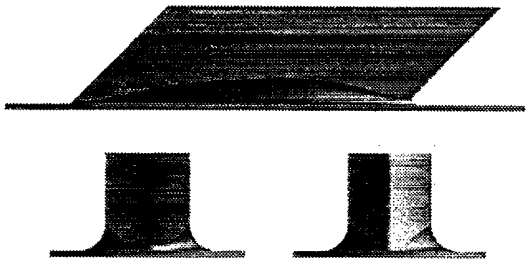

Figure 13: T/3-variable Fillet, Planar Hub

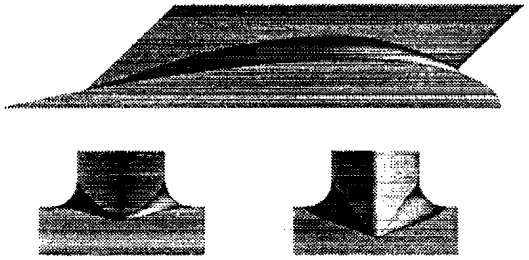

Figure 14: T/3-variable Fillet, NACA Hub

THE TEST FACILITY

The Cavitation Tunnel

Cavitation experiments on the test models were conducted in the cavitation tunnel located at the National Research Council's Institute for Marine Dynamics (Doucet 1992). Table 1 outlines the relevant capacities of the facility.

Test Section Dimensions	0.5 m x 0.5 m x 2.2 m
Maximum Water Speed	10.0 m/s
Test Section Pressures	0.1 - 2.0 atm.

Table 1: Cavitation Tunnel Capacities

Figure 15 shows the installation of the apparatus in the tunnel. The mounting apparatus was attached to the forward top window of the test section. The test samples were mounted to the fixture by placing them under the apparatus and bolting up through the sample into the fixture. Each fillet was marked with numbered rows (Horizontally) and columns, at constant blade section chord fraction, as shown in Figure 15. These allowed the location of cavitation to be readily identified. In this paper we differentiate between X/C = 0.0, the location of the leading edge of the blade section prior to fitting the fillet, and L.E., the leading edge of the fillet.

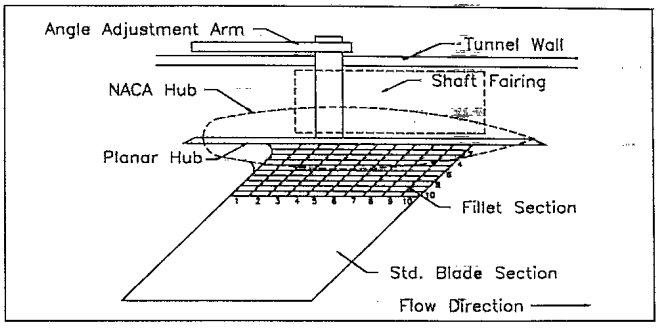

Figure 15: Test Apparatus

Measurement of Test Conditions

Tunnel test section pressures were measured with a mercury manometer connected to an orifice in the test section. The velocity, V, in the tunnel test section was calculated from the pressure difference between the upstream and downstream sections of the tunnel. A pitot tube was installed in the top of the tunnel to provide an additional velocity measurement. This was found to be redundant and all data in the paper are based on velocities calculated from the tunnel pressure differences.

Water Quality

Cavitation at full scale occurs in water that is saturated with gas. As the ambient pressure in the tunnel test section was reduced, the gas content of the water was also reduced proportionately to ensure that the water was neither highly supersaturated, resulting in premature cavitation, nor subsaturated, inhibiting cavitation. The gas content was regularly monitored and the tunnel water deaerated as required. Gas content was measured using a YSI Model 50B Dissolved Oxygen Meter with a YSI Model 5739 Field Probe.

Standard Cavitator

Since cavitation inception is highly affected by water quality and the test program was conducted over a period of several weeks, a standard cavitator was used in the tunnel to provide benchmark performance throughout the experimental program. This cavitator was a rectangular plan hydrofoil, mounted downstream of the model on the side wall of the tunnel. The foil has a span of 100 mm, a chord length of 33 mm and a NACA 0019 section shape. It was held in position by a mounting bracket from which a shaft protruded through the side of the tunnel. The shaft was attached to a calibrated quadrant that was used to set the angle of attack of the foil at $\theta = 10°$. A view of the standard cavitator is provided in Figure 16.

The conditions for tip vortex cavitation inception from the standard cavitator were measured as part of the test program for all but the T/3-variable fillet model. A

comparison of standard cavitator inception for each test allowed for assessment of the effect of water quality variability on the experimental results.

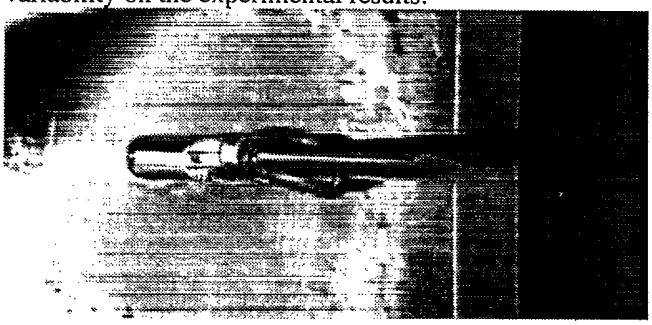

Figure 16: View of Standard Cavitator

Test Procedure

For both the planar and NACA hub series, the target gas content of the test water was chosen to be $\alpha/\alpha_S = 0.45$. The gas content was measured prior to each test. If the gas content was not sufficiently near the target, then the test water was further deaerated. When the measured gas content was within 10% of the target value, then the test was conducted at a target test section pressure ratio, P/P_{Atm}, equal to the actual gas content ratio.

The angle of attack of each test model was initially set at $\theta = 7°$, the angle at which the cavitation inception velocity should be lowest. Flow speed was increased from zero until the visual cavitation inception point was reached. All relevant parameters at inception were then measured.

The tunnel flow velocity was slowly reduced to the desinence point, where relevant parameters were again measured. No compensation of tunnel vacuum was made for the reduced velocity since the variation in dynamic pressure between inception and desinence is small.

Cavitation inception and desinence were measured three times for each foil using that procedure. Following the final desinence test, the flow speed was increased, beyond inception, to a point where cavitation was fully developed. Measurements of the flow conditions were then made for the fully developed state and the test was brought to completion by reducing the tunnel velocity to zero.

This process was repeated for each subsequent angle of attack of five, three and zero degrees, in that order.

Cavitation Patterns

The cavitation inception point was considered to be reached when intermittent cavitation was apparent on the foil such that it could be seen by any viewer most of the time. The cavitation desinence point was considered to be reached when no cavitation was visible at the location of inception for a period of more than ten seconds. The cavitation pattern at inception was sketched and recorded on videotape. Fully developed cavitation, produced by increasing the flow speed to eliminate the intermittent nature of inception, was photographed, sketched and videotaped.

Figure 17 shows fully developed cavitation on fillet test model T/3-compound. Typically, inception occurred as bubble cavitation. Normally it occurred forward of the mid-chord position and on the fillet. In some situations, sheet cavitation was visible along the leading edge. Less common was scarf vortex cavitation, occurring generally in cases where the fillet design resulted in very small radii.

Figure 17: Typical Cavitation Patterns on Test Model T/3-compound at 5° Angle of Attack.

TEST RESULTS

As many fillet types were tested with both the planar hub and the NACA hub, it is not practical to describe each test in complete detail. Rather, the tests on the T/3-compound fillet type are described completely for both hub types. The relative performance of the fillet types is then compared. These comparisons are made on the basis of mean cavitation inception number, σ_i. From a propeller designer's point of view, higher cavitation numbers are bad as they denote lower cavitation inception speeds.

In addition, some comparisons are made between the types and locations of cavitation at inception at an angle of attack, θ, of 5°. That angle represents a reasonable operating condition at a propeller root. To aid in the descriptions of the cavitation locations, reference should be made to Figures 15 and 17 which illustrate the grid pattern that was marked on each of the foils.

Planar Hub Data

There was little variability among the three cavitation inception values measured for any setup with the planar hub. Similarly, there was minimal variability among the three desinence values. Figure 18 shows the measurements from the T/3-compound fillet test. The mean values of the cavitation numbers are plotted as symbols, and the range of values indicated through the use of error bars. The lines on the plot are the mean inception and desinence points for vortex cavitation shed from the edge of the NACA 0019 standard cavitator.

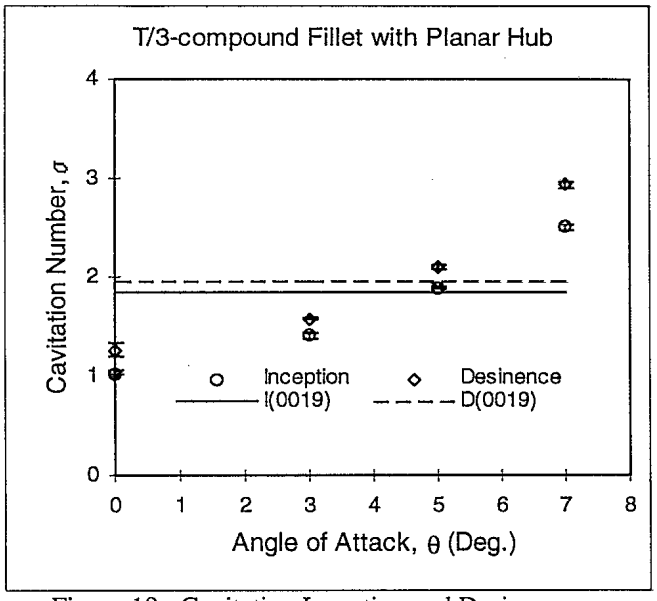

Figure 18: Cavitation Inception and Desinence on T/3-compound Fillet with Planar Hub

The data presented in Figure 18 are typical of those found from all the test models. The inception and desinence conditions were found to adequate precision to define the trends with angle of attack. Only one tenth of all the cavitation data from planar hub models had variations from the mean exceeding 5%. Additionally, the variation in cavitation inception on the NACA 0019 standard cavitator was within ±6.2% for all tests using the planar hub. The desinence data tracked the inception data well. Either inception or desinence could therefore be used in comparisons among test models. We chose to use cavitation inception.

The locations and types of cavitation at inception for the T/3-compound fillet with the planar hub are summarized in Table 2. At $\theta = 0°$ intermittent bubble cavitation began in the region from 0.2 to 0.5 chord and extended from rows 3 to 9. At $\theta = 3°$ both intermittent bubble and scarf vortex cavitation began in the region from the leading edge to 0.2 chord and extending from rows 3 to 6. The affected area was smaller than at $\theta = 0°$ and was shifted towards the leading edge (L.E.) of the fillet. At $\theta = 5°$, bubble cavitation began in the region from the leading edge to 0.1 chord and between rows 2 and 4. At $\theta = 7°$ the cavitation was at approximately the same location as for $\theta = 5°$, but the affected area was slightly smaller. Strictly speaking, bubble cavitation formed first, however, this immediately developed into sheet cavitation when the flow velocity was increased beyond inception.

θ	σ_i	Cavitation Type	Location X/C
0°	1.03	Bubble	0.2 - 0.5
3°	1.40	Bubble & Vortex	L.E. - 0.2
5°	1.88	Bubble	L.E. - 0.1
7°	2.51	Bubble & Sheet	L.E. - 0.1

Table 2: Cavitation Inception for Fillet T/3-compound with Planar Hub

Comparison of Single Radius Fillets

Four single radius fillet models, T/2, T/3, T/4 and No fillet, were tested with the planar hub. Figure 19 shows their relative performance in terms of cavitation inception. The No fillet model had the highest cavitation inception number over a broad range of angles of attack. It was clearly the least desirable. At high angles of attack the T/2 model cavitated at low speeds because of the sharp leading edge on the fillet radius. There was little difference in performance between the T/3 and T/4 models except at the highest angle of attack. At that angle the T/4 fillet performed the best.

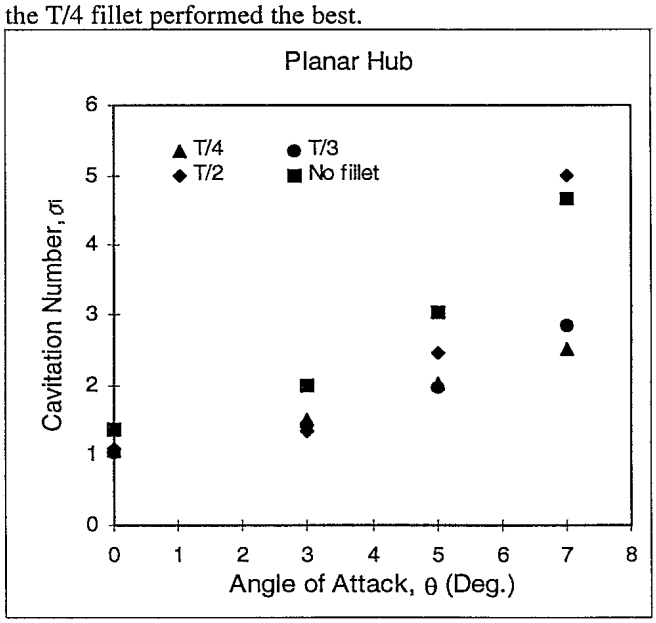

Figure 19: Cavitation Inception on Single Radius Fillets with Planar Hub

At $\theta = 5°$ the principal differences in cavitation inception among the fillets were quite apparent. For the No fillet model, cavitation was in the form of a fine vortex which extended from the leading edge to 0.1 chord, immediately adjacent to the hub. For the T/2 model, the cavitation was in the form of very fine bubbles exactly at the leading edge of rows 3 and 4. As noted earlier, this fillet had a knife-like leading edge, caused by the large fillet radius wrapping around on itself. For both the T/3 fillet and the T/4 fillet, cavitation was in the form of intermittent, isolated bubbles, located in rows 3 and 4

between 0.0 chord and 0.1 chord. The locations and types of cavitation at $\theta = 5°$ are summarized in Table 3

Fillet Type	σ_i	Cavitation Type	Location X/C
T/2	2.46	Fine Bubbles	L.E. exactly
T/3	1.98	Bubble	0.0 - 0.1
T/4	2.03	Bubble	0.0 - 0.1
No fillet	3.04	Vortex	L.E. - 0.1

Table 3: Cavitation Inception at $\theta = 5°$ for Single Radius Fillets with Planar Hub

Comparison Between Compound and Single Radius Fillets

In addition to the T/3-compound fillet that was described above, a T/4-compound fillet was also tested. The performance of these two fillets, and of the T/3 and T/4 fillets, are compared in Figure 20.

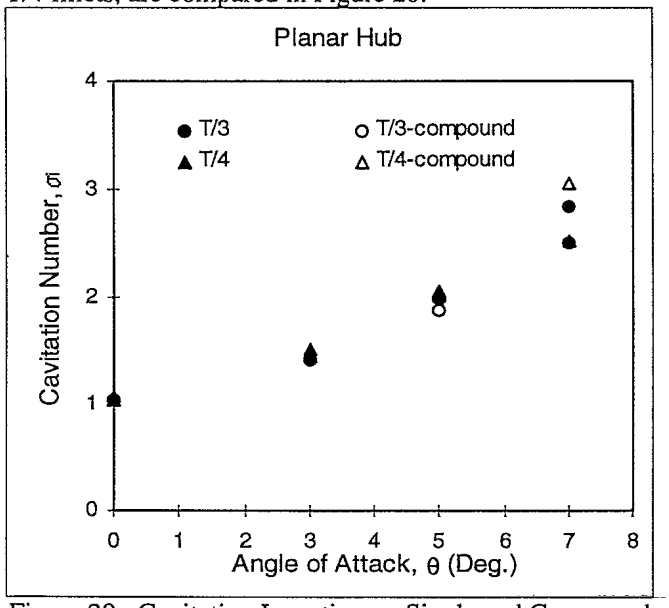

Figure 20: Cavitation Inception on Single and Compound Radius Fillets with Planar Hub

There is negligible difference between the four fillets at angles of attack up to $\theta = 5°$. At $\theta = 7°$, the T/3-compound and T/4 fillets provided the best performance while T/4-compound was the least desirable.

At $\theta = 5°$, cavitation inception for the T/4-compound fillet was in the form of bubbles which extended from the leading edge to 0.1 chord and was observed primarily in rows 2 and 3. In this regard the compound radius fillets were similar to each other, and somewhat different from the single radius fillets. Table 4 summarizes the locations and types of cavitation at $\theta = 5°$.

Fillet Type	σ_i	Cavitation Type	Location X/C
T/3	1.98	Bubble	0.0 - 0.1
T/3-compound	1.88	Bubble	L.E. - 0.1
T/4	2.03	Bubble	0.0 - 0.1
T/4-compound	2.05	Bubble	L.E. - 0.1

Table 4: Cavitation Inception at $\theta = 5°$ for Single and Compound Radius Fillets with Planar Hub

Comparison of Fillets Based on T/3

Four fillet models, T/3, T/3-compound, T/3-elliptic, and T/3-variable, were based on the dimension "T/3". The relative performance of these fillets was compared in Figure 21. The T/3-variable model had the highest cavitation number over a wide range of angles of attack. It was clearly the least desirable. The T/3-elliptic model had consistently higher cavitation numbers than the T/3-compound model over the whole range of operating angles. The T/3-compound fillet demonstrated the best performance overall.

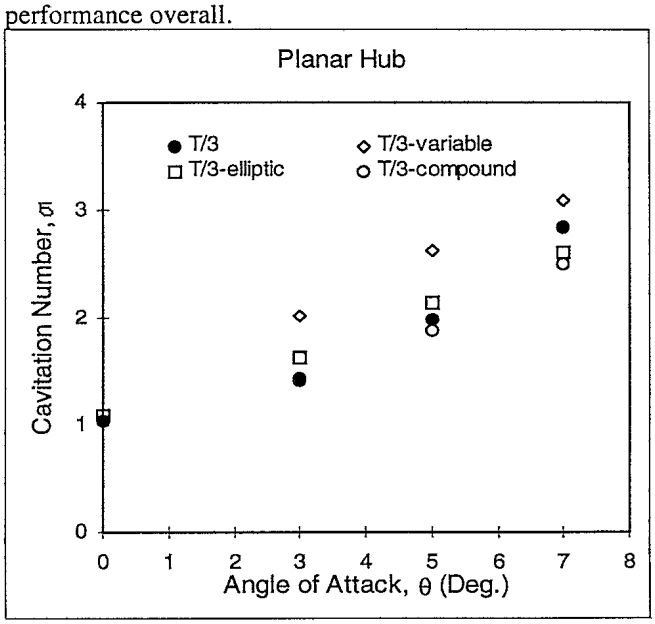

Figure 21: Cavitation Inception on Fillets Based on "T/3" with Planar Hub

For both the T/3-elliptic and the T/3-variable models, cavitation inception at $\theta = 5°$ occurred as a fine vortex extending from the fillet leading edge to 0.0 chord in row 1, i.e. at the intersection of the hub with the blade. The locations and types of cavitation inception are summarized in Table 5.

Fillet Type	σ_i	Cavitation Type	Location X/C
T/3	1.98	Bubble	0.0 - 0.1
T/3-compound	1.88	Bubble	L.E. - 0.1
T/3-elliptic	2.13	Vortex	L.E. - 0.0
T/3-Variable	2.63	Vortex	L.E. - 0.0

Table 5: Cavitation Inception at $\theta = 5°$ for Fillets Based on "T/3" with Planar Hub

NACA Hub Data

As with the planar hub tests, there was little variability among the three cavitation inception values measured for any setup with the NACA hub. Similarly, there was minimal variability among the three desinence values. Figure 22 shows the measurements from the T/3-compound fillet test. The mean values of the cavitation numbers are plotted as symbols, and the range of values indicated through the use of error bars. The lines on the plot are the mean inception and desinence points for a cavitating vortex shed from the edge of the NACA 0019 standard cavitator.

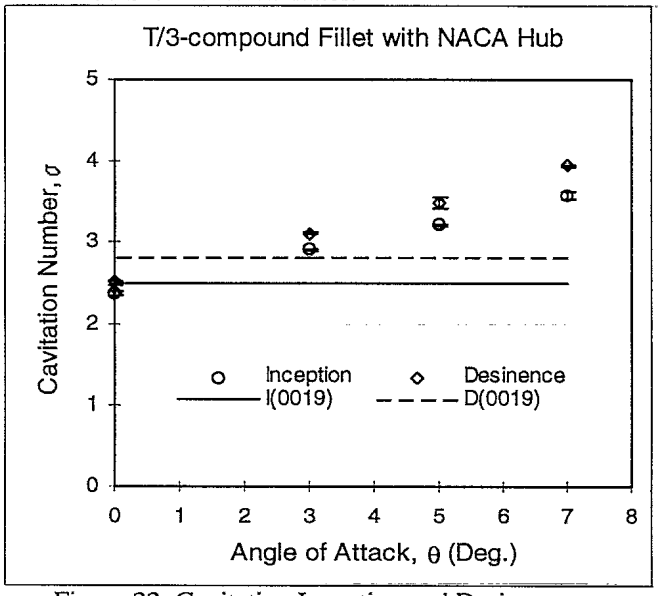

Figure 22: Cavitation Inception and Desinence on T/3-compound Fillet With NACA Hub

The results seen in Figure 22 are typical of those found from all the test models with the NACA hub. None of the data from NACA hub models had variations from the mean exceeding 3%. Additionally, the variation for cavitation inception on the NACA 0019 standard cavitator was within ±2%.

It should be noted that the standard cavitator inception and desinence data measured with the NACA hub are significantly different from those measured during the planar hub tests. This difference was partly due to the presence of the NACA hub, affecting the flow at the standard cavitator. Also, as there was one month between the planar and NACA hub tests, other unknown changes may have taken place. It was therefore not possible to unequivocally compare the planar hub cavitation data to the NACA hub data.

The locations and types of cavitation at inception for the T/3-compound fillet are summarized in Table 6. For all test angles, cavitation inception was in the form of intermittent bubbles. At $\theta = 0°$, cavitation began in rows 5 to 7 from 0.1 chord to 0.4 chord. At $\theta = 3°$, a smaller area was affected: cavitation was predominant in rows 5 and 6 from 0.1 chord to 0.3 chord. At $\theta = 5°$ the cavitating region shifted farther forward, with cavitation occurring in rows 5 and 6 from 0.0 chord to 0.2 chord. At $\theta = 7°$ the cavitating region was similar to that for $\theta = 5°$.

θ	σ_i	Cavitation Type	Location X/C
0°	2.36	Bubble	0.1 - 0.4
3°	2.91	Bubble	0.1 - 0.3
5°	3.22	Bubble	0.0 - 0.2
7°	3.57	Bubble	0.0 - 0.2

Table 6: Cavitation Inception for Fillet T/3-compound with NACA Hub

Comparison of Various Fillets

Three fillet models, T/3, T/3-compound, and T/3-variable, and one No fillet model were tested with the NACA hub. The relative performance of these fillets was compared in Figure 23.

The No fillet model had the highest cavitation number over the whole range of angles of attack. It was clearly the least desirable. At $\theta = 7°$ the T/3-variable model had a marginally higher cavitation number than the T/3-compound model. Otherwise there was no significant difference between the fillet types.

At $\theta = 5°$, there was bubble cavitation at inception for all the fillets. For the T/3 and the T/3-compound fillets, cavitation occurred from 0.0 chord to 0.2 chord in rows 5 and 6, i.e. fairly close to the intersection with the NACA hub. For the T/3-variable fillet the same rows were affected, but over a smaller area, as the cavitation was located from 0.1 chord to 0.2 chord. For the No-fillet model, bubble cavitation occurred at the intersection between the hub and the foil around 0.1 chord. The locations and types of cavitation at $\theta = 5°$ are summarized in Table 7.

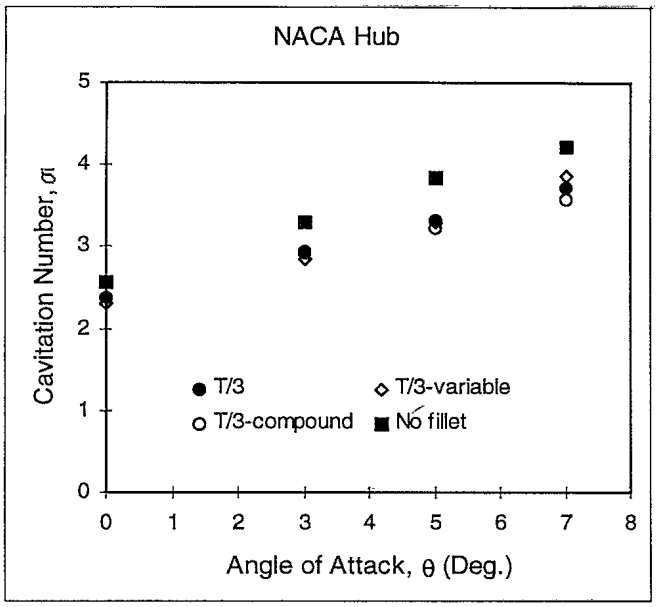

Figure 23: Cavitation Inception on Various Fillets with NACA Hub

Fillet Type	σ_i	Cavitation Type	Location X/C
T/3	3.31	Bubble	0.0 - 0.2
T/3-compound	3.22	Bubble	0.0 - 0.2
T/3-variable	3.30	Bubble	0.1 - 0.2
No fillet	3.84	Bubble	0.1

Table 7: Cavitation Inception at $\theta = 5°$ for Various Fillets with NACA Hub

OBSERVATIONS

The fillet sections on the NACA hub generally had higher cavitation numbers than their equivalent fitted to the planar hub. This was expected due to low pressures developed over the NACA hub shape. No quantitative comparison of hub shape effects could be made from the data presented here as the standard cavitator data suggests that test conditions may have changed between the tests on the two hub sets. Cavitation on the NACA hub fillets was found to be less sensitive to angle of attack than on the equivalent planar hub fillets. It was also noted that the NACA hub prevented cavitation inception from occurring exactly at the leading edge, for at all angles tested.

Results from all fillets showed that as the angle of attack was increased, the location of cavitation inception moved towards the leading edge and the area affected became smaller. This was the case for both hub shapes.

The fillets with small radii at the leading edge all performed badly. In the case of the planar hub, this was associated with vortex cavitation. In the case of the NACA hub, it was associated with a short line of bubbles. Also, the T/3-elliptic fillet, which performed rather poorly, had vortex cavitation. In all of these cases, the cavitation was adjacent to the hub.

CONCLUSIONS

We believe that the trends observed in these wing/body fillet tests will also apply to propeller blade root fillets.

Of all the fillets tested, the T/3-compound fillet was the best overall, but not by much. This fillet is difficult to construct and T/3 or T/4 single radius fillets gave similar cavitation inception results.

The critical area for cavitation inception was from the fillet's leading edge to 0.2 chord. This implies that the definition and inspection of the fillet are most important in that region.

Fillet shapes that give rise to vortex cavitation should be avoided. One such case is that of small radii. This presents a problem for controllable pitch propeller designers. They like to get as much of the blade root section as possible on the palm. To accomplish this they tend to specify small fillet radii at the leading edge. Fitting a large fillet radius at the leading edge has a significant impact on the structural design of the blades.

The presence of vortex cavitation on poorly performing fillets presents a problem for those who must vouch for propeller performance. Usually propeller cavitation performance is predicted by model test. However the relatively low Reynolds' Number of typical propeller model tests strongly affects vortex cavitation, and may not permit it to be observed. Model tests, similar to those conducted here, or computational fluid dynamic methods may have to be developed as alternative prediction methods.

REFERENCES

Doucet, J.M., "Cavitation Tunnel Instruction Manual", Report No. OERC92-TR-HYD-92005, Memorial University of Newfoundland, 1992.

Rules and Regulations for the Classification of Ships, Lloyd's Register of Shipping, 1982.

Rules for Classification of Steel Ships, Det Norske Veritas, 1983.

#503450